Neural Computing and Applications
https://doi.org/10.1007/s00521-021-05818-w

ORIGINAL ARTICLE

Neural network-based prediction for surface characteristics in CO_2 laser micro-milling of glass fiber reinforced plastic composite

Shashi Prakash[1] · Siddharth Suman[2]

Received: 2 July 2019 / Accepted: 10 February 2021

Abstract
A novel approach to predict the surface characteristics, namely depth and surface roughness, of glass fiber reinforced plastic composite after CO_2 laser milling by using artificial neural networks is developed and optimized. The experimental data are produced using a 60 W CO_2 laser machine to perform milling of unidirectional glass fiber reinforced plastic composite. The CO_2 laser milling is performed in both parallel and perpendicular to fiber direction at five different values of energy deposition (0.066, 0.176, 0.22, 0.264, 0.308) J/mm and three different beam diameters (225, 277.398, 463.869) μm. The artificial neural network model having the architecture of 3-6-6-3, that is two hidden layers with six neurons in each layer, is found to have the best performance based on mean error value. The mean, maximum, and minimum prediction errors for this ANN model are 0.82%, 2.26%, and 0.0004%, respectively. A semiempirical model is also developed to predict the milling depth, and its response is compared with predicted depth from neural network model. The milled depth predicted using the optimized neural network model is far superior compared to the output of the semiempirical model.

Keywords GFRP · ANN · Machine learning · Machining · Roughness

1 Introduction

Glass fiber reinforced plastic (GFRP) composite consists of glass fibers and plastic. The glass fibers provide mechanical reinforcement, while the plastic as resin is selected according to application. GFRP offers the advantage of high specific strength, better fatigue life, dimensional stability at extreme temperatures, corrosion resistant, fire resistant, etc [1]. Owing to all these properties, GFRP finds application in different industries like aerospace, marine, railway transport, defense, construction, etc [2]. On the one hand, the combination of glass fibers and plastic enables GFRP to exhibit the best properties of both materials, while on the other hand, this gives heterogeneous structure to GFRP which makes its machining very difficult [3]. Because of anisotropic nature and heterogeneous structures of GFRP, its machining with conventional machining process often results in failures such as resin cracking, fiber pull-out, and delamination [3–5]. Moreover, rapid tool wear due to the difference in mechanical properties of fiber reinforcement and plastic matrix also poses a great difficulty during conventional machining [2]. Various unconventional machining processes like water jet machining, ultrasonic machining, laser beam machining have been applied for GFRP machining. Electro-discharge machining is not an option for GFRP as glass fiber is not an electrical conductor. Even though water jet machining and laser beam machining are incorporated in industry for GFRP machining, these two processes have their own challenges. Water jet machining has the possibility of causing delamination of GFRP, while laser beam machining induces heat-affected zone in it. However, there is a risk of reduction in the strength of materials during water jet machining due to the absorption of water in the material [2, 5]. Laser beam machining has emerged as the suitable choice for machining of composites like GFRP as it results in higher productivity, better cut quality, and higher precision.

✉ Siddharth Suman
s.suman@iitp.ac.in

[1] School of Engineering and Applied Science, Ahmedabad University, Ahmedabad, Gujarat, India

[2] Nuclear Energy and Safety Research Division, Paul Scherrer Institute, 5232 Villigen, Switzerland

Published online: 06 March 2021

Research works surveying application of laser for machining of GFRP are given in Table 1. The features of the heat-affected zone induced in GFRP printed circuit boards during a UV YAG laser-drilled hole were investigated by Yung et al. [6]. It was found that drilling with lower power of laser in a repetition gives a clear hole wall with almost no black charred material. The structures of the HAZ produced by different laser parameters were analyzed. However, on drilling with high power and repetition rate, matrix recession and fiber protrusion were observed, also a loose coating was found covering the protruded glass fibers. Recently, Solati et al. [7] performed an extensive investigation of drilling in GFRP using CO_2 laser in contrast to UV YAG laser of Yung et al. [6]. Different combinations of laser parameters, cutting speed, and gas pressure were used in order to achieve minimum surface roughness, heat-affected zone, ovality, and maximum tensile strength of specimens after laser drilling. They also carried out the conventional drilling using 6-mm brad and spur drill bit on a computer numerical control machining center for comparison. It is reported that surface roughness and heat-affected zone is strongly dependent on laser intensity and cutting speed while ovality is mainly controlled by intensity of laser. Another important finding of this study is that tensile strength of laser-drilled GFRP laminate has linear dependency with heat-affected zone. Nevertheless, tensile strength is 1.3% higher, and surface roughness improved from 5.35 to 3.1 μm as compared to the traditional drilling method. Since no analytical model is available to predict heat-affected zone in laser drilling of GFRP, evaluation of tensile strength is also not possible. Based on their experimental data, Solati et al. [8] adopted combined genetic algorithm–artificial neural network approach to predict heat-affected zone and bearing strength in laser drilling of GFRP. The deviation in predicted values for both heat-affected zone and tensile strength was less than 2%. Fatimah et al. [9] conducted CO_2 laser cutting of GFRP to evaluate the effects of focused beam diameter on profile depth and material removal rate. The focus beam parameter of laser cutting affects the depth, material removal rate and surface quality. Choudhury and Chuan [1] used a continuous mode low power CO_2 laser for cutting of GFRP and investigated the effects of nozzle diameter, cutting speed, and number of laser beam pass on roughness and kerf width. Double-pass laser beam produced better surface appearance in terms of severity of burning and lower kerf width, while single-pass beam yielded lower surface roughness. Smaller nozzle diameter gives better

Table 1 Summary of research on laser machining of glass fiber reinforced plastic composite

References	Laser	Sample	Process	Highlights of the research
[6]	Nd:YAG	Reinforcement: glass; matrix: epoxy; thickness: 1.6 mm clad with 18 μm copper	Drilling	Structures of heat affected zone produced by different laser parameters are analyzed
[9]	CO_2	Reinforcement: e-glass; matrix: epoxy resin; thickness: 2.5 mm	Cutting	Effects of focal length on cut quality in terms of material removal rate and focus spot size
[1]	CO_2	Reinforcement: glass; matrix: polyester resin	Cutting	Assessment of cut surface quality by single-pass and double-pass Dependence of kerf width and surface roughness on laser parameters
[10]	CO_2	Reinforcement: roving glass; matrix: polyamide 6; thickness: 1 mm	Cutting	Continuous mode and pulsed mode are investigated Single-pass and multi-pass are compared
[37]	CO_2	Reinforcement: glass; thickness: 3 mm	Trimming	Variations in material removal rate, kerf angle, and surface roughness with laser parameters are investigated
[11]	Fiber	Reinforcement: e-glass; matrix: polyester resin; thickness: 5 mm	Cutting	Effects of laser cutting parameters on kerf width Kerf width increases with an increase in laser power and gas pressure
[12]	Fiber	Reinforcement: e-glass; matrix: polyester resin; thickness: 5 mm	Cutting	Effects of laser cutting parameters on heat affected zone ANN modeling of heat affected zone with mean error of 0.51%
[13]	Fiber	Reinforcement: e-glass; matrix: epoxy resin; thickness: 4.56 mm	Cutting	Dependence of Kerf width and heat affected zone on laser parameters
[7]	CO_2	Reinforcement: glass; matrix: epoxy; thickness: 1.2 mm	Drilling	Effects of laser parameters on surface roughness, heat-affected zone, and taper angle are evaluated
[8]	CO_2	Reinforcement: glass; matrix: epoxy; thickness: 1.2 mm	Drilling	Prediction of heat-affected zone and bearing strength using coupled genetic algorithm and artificial neural network

surface finish and lower kerf width. Effects of continuous mode and short-pulsed mode of CO_2 laser during cutting of GFRP in single-pass and multi-pass were studied by Schneider et al. [10]. They concluded that use of multi-pass processing at high cutting speed of 100 m/min confines the heat-affected zone in the range of 100 to 200 μm. Patel et al. [11] used fiber laser in continuous mode for cutting of GFRP and used experimental data to develop different predictive models for estimating the kerf width. On comparison of predicted responses obtained from second-order regression, artificial neural network, and fuzzy logic, it was concluded that model based on fuzzy logic has the least mean error. Later, Patel et al. [12] developed similar models to predict the size of heat-affected zone during the cutting of GFRP using fiber laser and reported that artificial neural network model has the best prediction results. Rao et al. [13] also used continuous-mode fiber laser to cut GFRP and investigated effects of processing parameters, namely laser intensity, cutting speed, gas pressure on cut surface quality. Based on the experimental data, they optimized the process parameters using response surface methodology. The confirmation experiments at the optimized parameters produced kerf width and heat-affected zone within 2.52% and 0.45%, respectively.

Based on this succinct literature review, it was concluded that there is a lack of investigation of milling process of GFRP using laser. Moreover, most of studies discuss the prediction of geometric characteristics rather than surface roughness. Given the lack of understanding about laser beam interaction with anisotropic GFRP, there is no analytical model to predict the milled depth. A possible solution to model such complex process lacking clear theoretical understanding is the adoption of cognitive systems and in particular the artificial neural network. Although artificial neural networks also show some drawbacks like requirement of large number of experimental data points or need of many trials to select suitable network architecture, they are quite powerful in finding functional relationships among different inputs/outputs by learning from examples. Since neural network learns by examples, there is neither requirement of a deep knowledge on the process mechanisms like in case of an empirical model or finite element modeling nor it is restricted to use of defined mathematical relation among independent and response variables like in analysis of variance or response surface methodology. Moreover, different researchers [11, 14] have reported superior performance of artificial neural networks for prediction of machining parameters of anisotropic material using laser. Thus, the objectives of present study are to conduct CO_2 laser milling of GFRP and to develop an optimized artificial neural network for prediction of milled depth and surface roughness.

2 Experimental investigation

The laser milling tests are performed on GFRP composite (supplied by Arvind PD composites, India) having E-type glass fibers as reinforcement and epoxy resin as matrix. Glass fibers having diameter in the range of 7–12 μm are laid unidirectional, and its volume percentage is approximately 35%. No colorant is added to the epoxy, and the color of the sample is creamy white as shown in Fig. 1. The magnified microscopic inset in Fig. 1 clearly shows the fibers and resin.

A 60-W CO_2 laser machine (Trotec, Speedy 100, Austria) is used in continuous mode to mill GFRP. The milling is performed for three different beam diameters (225 μm, 277.398 μm, 463.869 μm), and it is achieved by varying the focusing distance. Energy deposition by a laser beam is ratio of beam power to scanning speed, and milling is done at five different energy deposition (0.066, 0.176, 0.22, 0.264, 0.308) J/mm. To investigate the directional effects since the GFRP is anisotropic in nature, the milling is performed in two different directions, namely milling with laser beam movement parallel to fiber direction and milling with laser beam movement perpendicular to fiber direction; a schematic is shown in Fig. 1. A total sixty experiments are conducted with three different beam diameters, five different energy levels, and two different directions of milling according to full factorial design, where repeatability is kept 2. Milled area is kept 10 mm × 10 mm. Pulse per inch is fixed at 1000 in linear direction and 500 in lateral direction, that is 89% of linear overlapping and 79% of vertical overlapping, for all the experiments. The pulse per inch values do not have any significant effect on milled depth as the total energy deposition remains constant

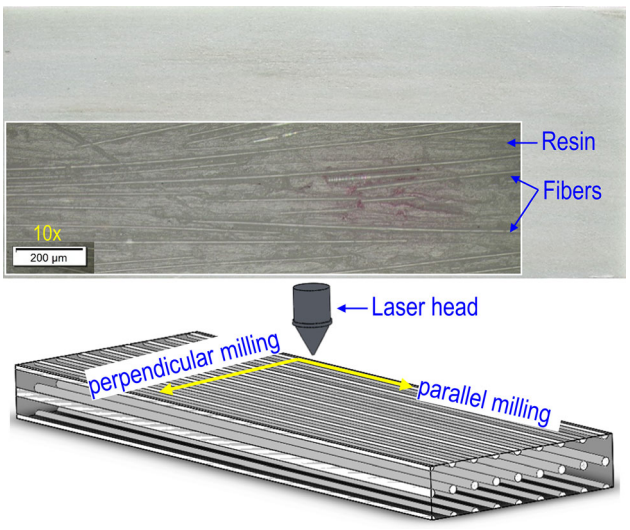

Fig. 1 Structure of as-received GFRP and schematic of its laser micro-milling

during milling in both parallel and perpendicular to fiber directions. Milled depth and surface roughness are measured as outputs. Details of experimental results are given in Table 2.

2.1 Milling depth

The milled depth is measured using an optical microscope at three different locations, and the average value is taken as final depth. The variation in milled depth with energy deposition during milling parallel to fiber direction and perpendicular to fiber direction for different beam diameters is shown in Figs. 2 and 3, respectively. For milling in both directions, namely parallel to fiber direction and perpendicular to fiber direction, the milled depth increases almost linearly with energy deposition. The milled depth decreases with an increase in beam diameter as larger beam diameter causes the spread of energy density at the focus spot of laser. It is also seen that for given beam diameter and energy deposition, the milled depth is higher in case of milling done along the fiber direction. Also for milling in both directions, the influence of beam diameter is more pronounced at higher energy deposition.

Energy transfer in composite materials is a complex phenomenon due to its heterogeneous or anisotropic nature. There is no clear or exact understanding of laser beam interaction with GFRP, and thus development of an analytical method to predict the milled depth during laser milling is still in research. However, a semiempirical model for depth prediction may be developed on the basis of models developed for single constituent polymers like poly(methyl methacrylate) or acrylic [15, 16]. For a polymeric material like PMMA, the laser ablation depth Z can be calculated as (for detailed derivation readers may refer [16]):

$$Z = \sum_{n=1}^{n} K_{\text{psm}} \frac{\alpha}{\rho\left(c_{\text{p}}\Delta T + H_{\text{L}}\right)} \sqrt{\frac{2}{\pi w^2}} \frac{P}{U} e^{\frac{-2[Y-(n-1)c_1]^2}{w^2}} \tag{1}$$

where K_{psm} is pulse smearing coefficient, α is absorptivity, ρ is density, c_{p} is specific heat, ΔT is difference between ambient temperature and vaporization point, H_{L} is latent heat of vaporization, w is beam radius, P is laser power, and U is scanning speed. n and c_1 are constants whose values are dependent upon number of strokes and pulse overlapping.

It is established that ablation depth is a function of beam radius w, thermo-optical properties of material, and energy deposition P/U. However, in case of composite materials like GFRP, the material properties do not remain same everywhere given their anisotropic nature, and thus milled depth can be written as:

$$\text{Milled depth} \propto f\left(w, \frac{P}{U}, K_{\text{psm}}\right) \tag{2}$$

Based on the regression analysis performed on experimental values obtained during the present study, milled depth is expressed in form of simple power law as:

$$\text{Milled depth} = g_1 \times \left(K_{\text{psm}} \times w \times \frac{P}{U}\right)^{g_2} \tag{3}$$

where g_1 and g_2 are experimental constants whose values are dependent upon milling directions, anisotropic behavior of GFRP used in this study. The value of K_{psm} is taken as 0.55 [16]. The value of experimental constants g_1 and g_2 obtained in this study is given in Table 3.

The developed empirical model is verified for different energy deposition and beam diameters for milling in both parallel and perpendicular to fiber directions. This model is also validated outside the experimental range of energy deposition by conducting additional tests at energy deposition of 0.40 J/mm and beam diameters of 225 μm and 463.869 μm. As shown in Fig. 4, the maximum percent deviation lies within ± 12%.

2.2 Surface roughness

Surface roughness of the milled pocket is measured in both directions, namely parallel to fiber directions and perpendicular to fiber directions, for each milled area. The variation in surface roughness with energy deposition during milling parallel to fiber direction and perpendicular to fiber direction for different beam diameters is presented in Figs. 5 and 6, respectively. For milling done parallel to fiber directions, surface roughness is greater in direction perpendicular to fiber direction for a given beam diameter. With an increase in energy deposition, the surface roughness decreases in direction parallel to fiber, while it increases in direction perpendicular to fiber for all beam diameters investigated. This may be because of better vaporization of resin and more breakage of fiber with an increase in energy deposition along the fiber direction. Similar trends in surface roughness are also observed for milling done perpendicular to fiber direction. For a given beam diameter and energy deposition, the surface roughness parallel to fiber direction is observed to be usually greater for milling done perpendicular to fiber direction. For same beam diameter and milling direction, milling depth increases with an increase in energy deposition. However, surface roughness also increases in both parallel and perpendicular to fiber directions. These may be because of more irregular vaporization of the GFRP during machining perpendicular to fiber direction, which is also confirmed by scanning electron microscopy, which is shown in Fig. 7. Figure 7 illustrates the effect of milling

Table 2 Results of experimental investigation

Sample ID	Energy deposition (J/mm)	Beam diameter (μm)	Milling direction (wrt fiber orientation)	Depth (μm)	Roughness	
					∥ to fiber (μm)	⊥ to fiber (μm)
#1	0.066	225.0	∥	70	5.84	8.34
#31	0.066	225.0	∥	67	4.95	8.20
#2	0.176	225.0	∥	196	4.74	8.58
#32	0.176	225.0	∥	201	5.60	7.34
#3	0.220	225.0	∥	270	4.15	9.88
#33	0.220	225.0	∥	272	4.20	8.95
#4	0.268	225.0	∥	349	3.70	10.10
#34	0.268	225.0	∥	338	4.10	10.35
#5	0.308	225.0	∥	400	3.27	10.82
#35	0.308	225.0	∥	408	3.20	9.60
#6	0.066	277.4	∥	57	5.77	7.29
#36	0.066	277.4	∥	61	6.20	8.10
#7	0.176	277.4	∥	172	4.66	8.02
#37	0.176	277.4	∥	168	4.32	7.38
#8	0.220	277.4	∥	226	3.93	8.86
#38	0.220	277.4	∥	228	4.10	7.64
#9	0.268	277.4	∥	291	3.49	9.63
#39	0.268	277.4	∥	278	3.30	9.56
#10	0.308	277.4	∥	343	3.18	9.89
#40	0.308	277.4	∥	340	3.16	9.92
#11	0.066	463.8	∥	50	5.60	6.90
#41	0.066	463.8	∥	56	6.20	7.10
#12	0.176	463.8	∥	152	4.65	7.83
#42	0.176	463.8	∥	137	4.60	6.75
#13	0.220	463.8	∥	205	4.33	8.10
#43	0.220	463.8	∥	203	3.76	9.24
#14	0.268	463.8	∥	239	3.44	8.41
#44	0.268	463.8	∥	242	3.40	7.89
#15	0.308	463.8	∥	293	2.22	8.85
#45	0.308	463.8	∥	287	2.86	9.2
#16	0.066	225.0	⊥	55	4.06	7.43
#46	0.066	225.0	⊥	59	3.79	8.10
#17	0.176	225.0	⊥	172	3.82	7.76
#47	0.176	225.0	⊥	181	4.12	8.40
#18	0.220	225.0	⊥	240	3.60	7.92
#48	0.220	225.0	⊥	242	3.47	7.65
#19	0.268	225.0	⊥	315	2.50	8.43
#49	0.268	225.0	⊥	304	2.32	8.80
#20	0.308	225.0	⊥	365	2.19	8.66
#50	0.308	225.0	⊥	357	3.10	7.95
#21	0.066	277.4	⊥	46	5.70	7.19
#51	0.066	277.4	⊥	48	5.20	7.20
#22	0.176	277.4	⊥	163	4.40	7.64
#52	0.176	277.4	⊥	178	5.20	9.20
#23	0.220	277.4	⊥	207	3.95	7.81
#53	0.220	277.4	⊥	215	4.10	6.89
#24	0.268	277.4	⊥	241	2.60	8.47

Table 2 (continued)

Sample ID	Energy deposition (J/mm)	Beam diameter (μm)	Milling direction (wrt fiber orientation)	Depth (μm)	Roughness	
					∥ to fiber (μm)	⊥ to fiber (μm)
#54	0.268	277.4	⊥	237	2.52	8.67
#25	0.308	277.4	⊥	318	2.36	9.08
#55	0.308	277.4	⊥	296	3.30	9.20
#26	0.066	463.8	⊥	40	7.27	8.13
#56	0.066	463.8	⊥	44	8.23	8.10
#27	0.176	463.8	⊥	135	5.33	8.61
#57	0.176	463.8	⊥	147	6.70	7.92
#28	0.220	463.8	⊥	197	6.29	8.75
#58	0.220	463.8	⊥	194	6.25	9.10
#29	0.268	463.8	⊥	232	4.53	8.98
#59	0.268	463.8	⊥	243	4.86	8.63
#30	0.308	463.8	⊥	286	4.07	9.95
#60	0.308	463.8	⊥	293	5.26	8.69

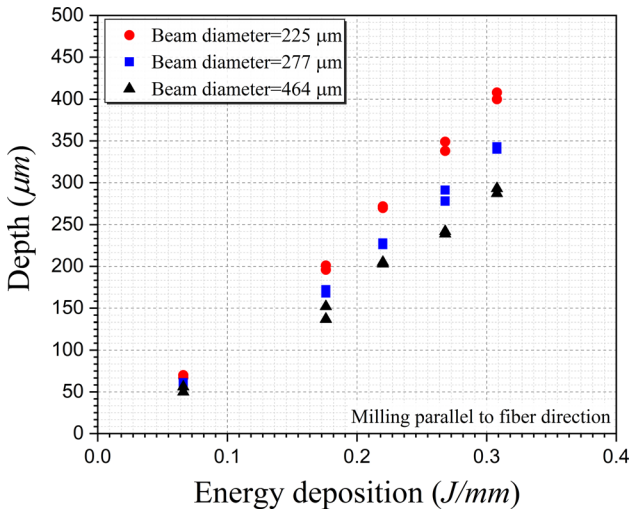

Fig. 2 Variation in depth with energy deposition for milling parallel to fiber direction

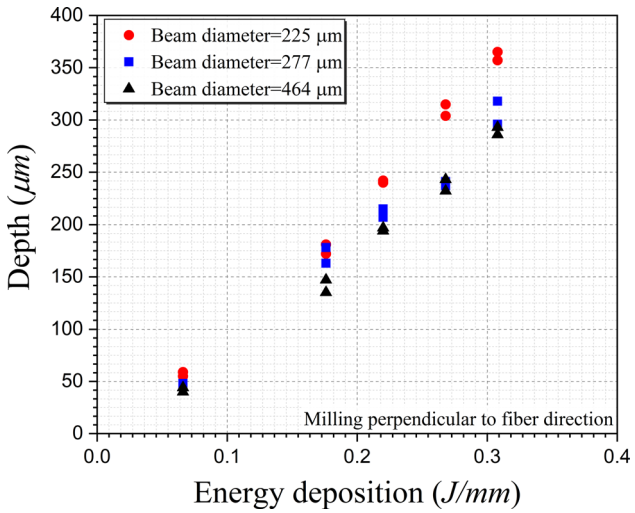

Fig. 3 Variation in depth with energy deposition for milling perpendicular to fiber direction

orientation and energy deposition value for a given beam diameter. Figure 8 shows effects of milling direction on surface roughness. Milling perpendicular to fiber direction produces rougher surface.

3 Development of artificial neural network model

An artificial neural network (ANN) structure essentially consists of layers and nodes (nodes are also known as neurons). Any ANN structure consists of three layers, namely input layer, hidden layer, and output layer. Hidden layer is the layer which establishes the functional relationship among inputs and outputs based on learning by the data. Neurons include inputs, weights, a summation function, an activation function, and outputs. The summation function is used to find the net input of the neuron as given in Eq. (4) [17–20]

$$\mathrm{NET}_i = \sum_{j=1}^{n} w_{ij} x_j + w_{\mathrm{bi}} \tag{4}$$

where NET_i is the weighted sum of the input to the i_{th} processing element, w_{bi} the weights of the biases between layers, x_j the output of the j_{th} processing element, w_{ij} the weights of the connections between i_{th} and j_{th} processing elements, i and j the processing elements, and n the number of processing elements in the prior layer.

Table 3 Values of experimental constants to predict the milled depth in GFRP

Beam diameter (μm)	Milling direction (wrt fiber orientation)	Constants	
		g_1	g_2
225.0	∥	11.47 ± 0.94	1.20 ± 0.029
	⊥	9.48 ± 0.83	1.24 ± 0.031
277.4	∥	7.69 ± 0.70	1.20 ± 0.030
	⊥	8.99 ± 2.21	1.11 ± 0.082
463.8	∥	4.34 ± 0.76	1.14 ± 0.049
	⊥	2.98 ± 0.45	1.24 ± 0.042

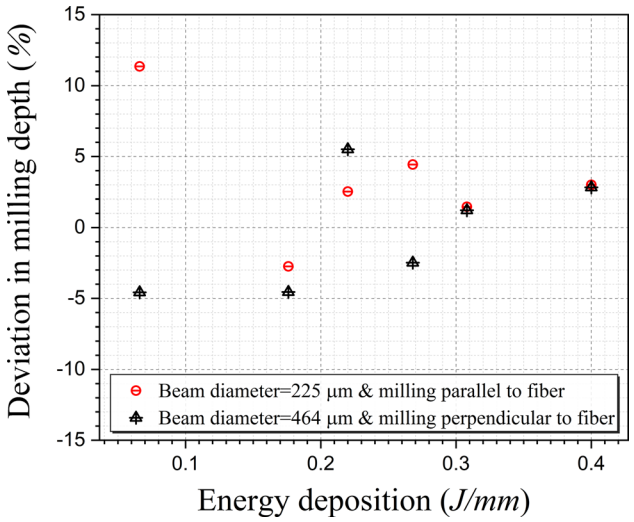

Fig. 4 Validation of semiempirical model developed to predict the milled depth of GFRP

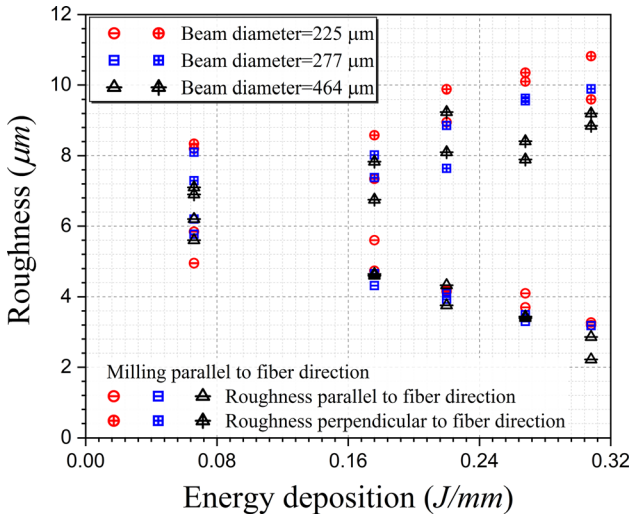

Fig. 5 Variation in surface roughness with energy deposition for milling parallel to fiber direction

Since the overall ANN architecture affects the predictive response, one of the issues of the present work is to develop an optimal ANN architecture. Some of the factors that can influence the effectiveness of ANN are as follows.

3.1 Network structure

The number of nodes in input layer and output layer is determined on the basis of number of input and output parameters, respectively. However, the number of hidden layers and the nodes in each hidden layer are dependent to the complexity of the input–output mapping, computational memory and time required to achieve the response. Too many hidden layers and nodes result in high computational cost, while too few nodes may not provide optimized results. Thus, the number of hidden layers and number of nodes in each hidden layer are decided on a trial-and-error basis to obtain the best results. Abeesh et al. [21] used ANN with 5-8-1 structure, meaning that it has five nodes for input layer, one hidden layer with eight nodes, and one node for output layers, for prediction of surface roughness. Grzesick and Brol [22] used the 7-72-72-72-7 structure, meaning that it has three hidden layers with seventy-two nodes in each layer. Kohli and Dixit [23] applied 4-3-1 structure, while Sanjay and Jyothi [24] used five different structures, 4-1-1, 4-5-1, 4-10-1, 4-15-1, and 4-20-1, to predict the surface roughness value and concluded that the 4-1-1 network structure yielded the best prediction for the surface roughness. In light of randomness of ANN structure used by different researchers to predict surface roughness after machining process, this study tests and compares the results of different ANN structure selected based on guidelines given by Zhang et al. [25]. They recommended that number of nodes in hidden layer should be $n/2$, n, $2n$, and $2n + 1$, where n is the number of nodes in input layer. Since number of nodes in input layer is equal to number of input variables which is three for this study, namely energy deposition, beam diameter, and direction of milling, the number of nodes in the hidden layer should be 1, 3, 6, and 7. Therefore, by limiting the trial-and-error process up to two hidden layers, this study applies eight different network structures, which are 3-1-3, 3-3-3, 3-6-3, 3-7-3, 3-1-1-3, 3-3-3-3, 3-6-6-3, 3-7-7-3.

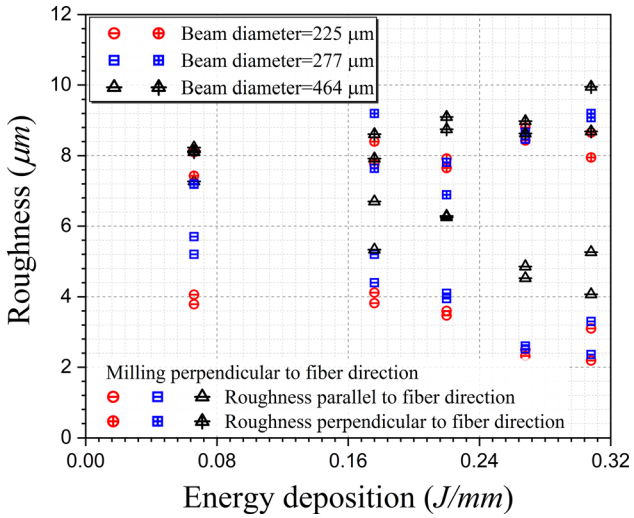

Fig. 6 Variation in surface roughness with energy deposition for milling perpendicular to fiber direction

3.2 Number of training and testing data

ANN is conceptually based on learning from data and thus larger the database for training the network, better is its prediction. In manufacturing and machining industries, data needed to train the ANN are generated from actual experiments. Many constraints such as the availability of material, cost, and time required for conducting the experiments exist for researchers in getting large number data for training. The amount of training and testing data collected by researchers varies from as low as 20 samples of data for training and ten samples of data for testing during developing ANN models with regard to predict the value of surface roughness [26]. Zuperl and Cus [27], Cus and Zuperl [28], Kohli and Dixit [23], Al-Ahmari [29], and Davim et al. [30] have obtained an accurate result for predicting surface roughness with total number of data 40, 30, 31, 28, 30, respectively. Thus, the dataset of 60 experiments in the present study is expected to provide an accurate predictive result for surface roughness using ANN, as reflected by results obtained in the previous work [23, 26–30].

To normalize the raw data of input and output, two potential normalization equations frequently used are [26]

$$x_i = \frac{2}{d_{\max} - d_{\min}}(d_i - d_{\min}) - 1 \tag{5}$$

$$x_i = \frac{0.8}{d_{\max} - d_{\min}}(d_i - d_{\min}) + 0.1 \tag{6}$$

$d_{\max}$ is the maximum value of the input/output data, $d_{\min}$ is the minimum value of the input/output data, and d_i is the ith input/output data. As a suggested solution [26], Eq. (6) is chosen for the normalization of the input/output data for this study.

3.3 Network algorithm and its components

Many different ANN algorithms have been proposed by researchers for modeling the response of a system such as cascade-forward backpropagation (BP), time-delay BP, Elman BP, radial basis, and feedforward BP. However, feedforward backpropagation algorithm is mostly applied by researchers for predicting surface roughness [22, 23, 26–30]. For example, Zuperl and Cus [27] developed ANN model using both feedforward BP and radial basis network algorithm, and it was established that the feedforward BP gave more accurate results. There are also different transfer functions available for ANN algorithm such as log-sigmoid transfer function (*logsig*), linear transfer function (*purelin*), hyperbolic tangent sigmoid transfer function (*tansig*), and hard limit transfer function (*hardlim*). There is no clear documentation in the literature about the selection of transfer function. Nalbant et al. [31] mentioned that the choice of transfer function is dependent on the nature of problem. Kohli and Dixit [23] applied both *logsig* and *tansig* transfer functions in their study, and concluded that both these transfer functions provided almost similar response. However, a number of studies usually applied *logsig* transfer function as it has an advantage that the output cannot grow infinitely large or small. The difference between the experimental output and predicted response of ANN model is error, and this error is measure of performance of the model. The error is referred as performance function, and there are different performance functions to evaluate an ANN model, for example mean square error (MSE), mean absolute error (MAE), sum of squares for error (SSE), root-mean-square of error (RMSE), mean absolute percentage error (MAPE), etc. Like the issue of transfer functions, there is no clarity provided by the literature regarding the selection of performance functions. However, most of the ANN models used for surface roughness prediction applied mean square error (MSE) performance function.

In light of aforementioned studies performed to predict surface roughness using ANN model during machining, this study applied feedforward backpropagation algorithm, *logsig* transfer function, and evaluated the model based on mean square error (MSE) performance function. The error during the learning called as mean squared error (MSE) is calculated as follows [17, 20, 32]:

$$\text{MSE} = \frac{1}{n}\sum_{i=1}^{n}(t_i - o_i)^2 \tag{7}$$

where t is target value, o is output value, and n is number of

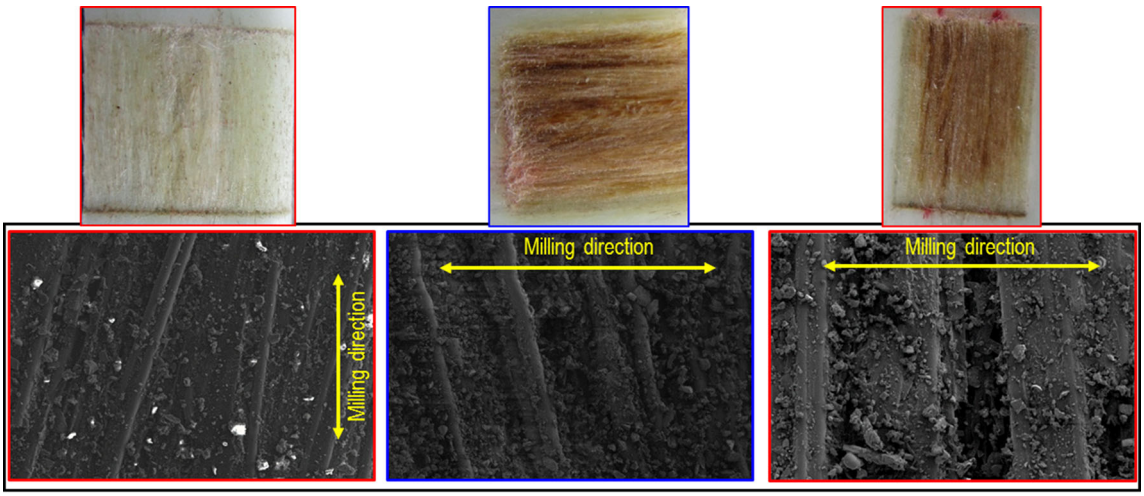

Fig. 7 SEM images showing the effects of energy deposition and milling direction

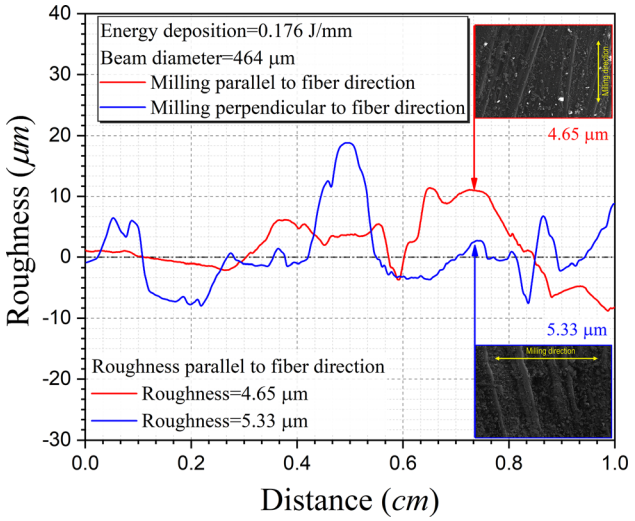

Fig. 8 A comparison of surface roughness parallel to fiber direction for a given beam diameter and energy deposition

samples. The weights between hidden layer and output layer are adjusted and are again calculated using the chain rule of differentiation as follows [33]:

$$\Delta w_{ji}(n) = \eta \delta_j(n) y_i(n) \tag{8}$$

$$\delta_j(n) = e_j(n)\varphi'\left(\sum_{i=0}^{m} w_{ji}(n) y_i(n)\right) \tag{9}$$

$$\delta_j(n) = \varphi'\left(\sum_{i=0}^{m} w_{ji}(n) y_i(n)\right) \sum_{k}^{m} \delta_k(n) w_{kj}(n) \tag{10}$$

$$\Delta w_{ji}(n) = \alpha \Delta w_{ji}(n-1) + \eta \delta_j(n) y_i(n) \tag{11}$$

where η is the learning rate parameter and α is the momentum coefficient.

4 Results and discussion

The mean prediction errors in percentage are calculated for each network structure as [34, 35]:

$$\%\ \text{mean prediction error} = \frac{1}{p}\sum_{1}^{p} \left(\frac{|\text{experimental value} - \text{predicted value}|}{\text{exprimental value}} \times 100\right) \tag{12}$$

The performance of all the ANN models is given in Table 4. Based on minimum mean error in the predicted response, the ANN model with two hidden layers having six nodes in each layer, shown in Fig. 9, is found to be the most suitable among all. The mean, maximum, and minimum prediction errors for this ANN model are 0.82%, 2.26%, and 0.0004%, respectively.

The results of this ANN model having 3-6-6-3 structure are only discussed hereafter.

Table 4 Performance of artificial neural network with different structure

ANN architecture (input–hidden–output)	Prediction error		
	Mean (%)	Maximum (%)	Minimum (%)
3-1-3	16.75	25.86	2.20
3-3-3	8.36	14.32	0.84
3-6-3	6.39	12.65	0.30
3-7-3	11.21	18.20	1.1
3-1-1-3	13.86	22.78	0.48
3-3-3-3	5.83	12.89	0.71
3-6-6-3	**0.82**	**2.26**	**4E−4**
3-7-7-3	2.13	18.32	0.20

Bold values indiacte the best or optimum network developed

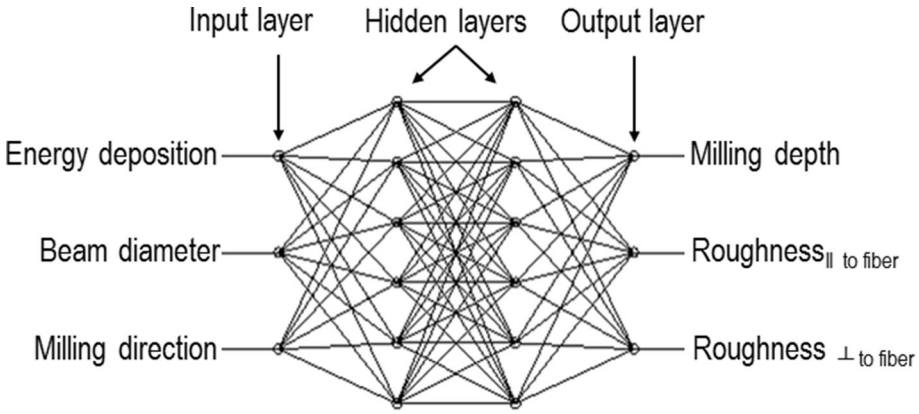

Fig. 9 An optimized backpropagation deep neural network (3-6-6-3) used for predicting micro-milled surface characteristics of GFRP

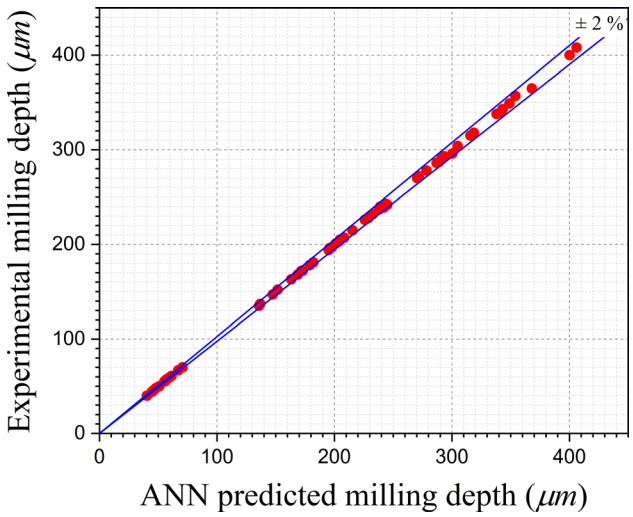

Fig. 10 Comparison of experimental milling depth with ANN model predicted depth

4.1 Milling depth

Figure 10 shows a comparison between experimental milling depth and ANN predicted milling depth. The predicted milled depth using ANN model has an excellent agreement with experimental value, and all the values for milled depth lie within ± 2%. Linear regression analysis is also performed to evaluate the coefficient of determination R^2 [35], and its value is found to be 0.999. The value of R^2 is almost equal to unity, and thus this ANN model is suitable for the prediction of milling depth of GFRP machined using CO_2 laser. A comparison of ANN model predicted milling depth is also performed with milling depth calculated using the empirical model, and the result is given in Table 5. As observed from Table 5, the results obtained from ANN model are far superior to results of empirical model.

4.2 Surface roughness

The predicted response obtained from the optimized ANN model for surface roughness in both parallel and perpendicular to fiber direction is plotted against corresponding experimental value in Figs. 11 and 12, respectively. The predicted surface roughness values lie within ± 2% for both directions. There is no analytical model to predict the surface roughness, and its prediction using ANN model with a reasonable accuracy establishes that surface roughness value as well as its directional dependence can be predicted using ANN model. The coefficient of

Table 5 Comparison of experimental milling depth with empirical model and ANN model

Sample ID	Energy deposition (J/mm)	Beam diameter (μm)	Milling direction (wrt fiber orientation)	Depth (with % deviation)		
				Experimental (μm)	Empirical (μm)	ANN (μm)
#1	0.066	225.0	∥	70	62.06 [11.33%]	70.64 [0.91%]
#2	0.176	225.0	∥	196	201.37 [2.74%]	195.80 [0.10%]
#3	0.220	225.0	∥	270	263.20 [2.52%]	270.32 [0.11%]
#4	0.268	225.0	∥	349	333.53 [4.43%]	348.96 [0.01%]
#5	0.308	225.0	∥	400	394.13 [1.46%]	400.12 [0.03%]
#26	0.066	463.8	⊥	40	41.82 [4.57%]	40.36 [0.90%]
#27	0.176	463.8	⊥	135	141.14 [4.55%]	135.85 [0.62%]
#28	0.220	463.8	⊥	197	186.14 [5.51%]	197.89 [0.45%]
#29	0.268	463.8	⊥	232	237.75 [2.48%]	232.56 [0.24%]
#30	0.308	463.8	⊥	286	282.51 [1.22%]	286.96 [0.33%]

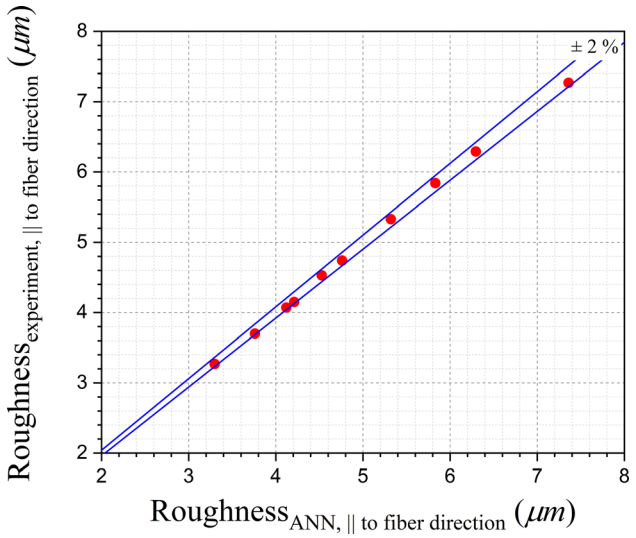

Fig. 11 Comparison of experimental surface roughness with ANN model predicted surface roughness in parallel to fiber direction

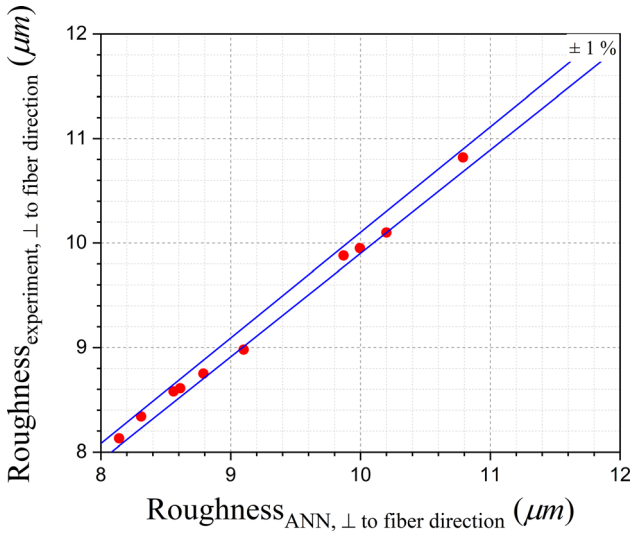

Fig. 12 Comparison of experimental surface roughness with ANN model predicted surface roughness in perpendicular to fiber direction

determination R^2 is 0.997 and 0.993 for surface roughness parallel and perpendicular to fiber during milling, respectively.

It is known that quality of approximation for neural network may be highly influenced by use of different activation functions. Although the optimized neural network with logsig transfer function predicted the milling depth and surface roughness quite well, the present research can be further extended with more complex activation functions like scaled polynomial constant unit (SPOCU) activation function [36] which works well on a variety of problems.

5 Conclusions

A 60-W CO_2 laser machine is used in continuous mode to perform micro-milling of unidirectional glass fiber reinforced plastic composite. The milling is done at five different energy deposition values (0.066, 0.176, 0.22, 0.264, 0.308) J/mm, three different laser beam diameters, and in both parallel and perpendicular to fiber direction. The milling depth and surface roughness in both parallel and perpendicular to fiber direction are evaluated after the test. Few samples are also examined under scanning electron microscope to have better understanding of input parameters. A semiempirical model is also developed to predict the milled depth, and its predicted response lies within ± 12%.

To predict the milled depth and more importantly surface roughness of GFRP after milling, an optimized artificial neural network model is developed. The ANN model having the architecture of 3-6-6-3, that is two hidden layers with six neurons in each layer, is found to have the best performance based on mean error value. The mean, maximum, and minimum prediction errors for this ANN model are 0.82%, 2.26%, and 0.0004%, respectively. The milled depth predicted using this ANN model is far better compared to output of the semiempirical model. The predicted values of surface roughness in both parallel and perpendicular to fiber direction show an excellent agreement with experimental values, and the predicted values lie within $\pm$ 2%.

Funding This research did not receive any specific grant from funding agencies in the public, commercial, or not-for-profit sectors.

Declarations

Conflict of interest The authors declare no known potential conflicts of interest with respect to financial interests or the research, authorship, and publication of this article.

References

1. Choudhury IA, Chuan PC (2013) Experimental evaluation of laser cut quality of glass fibre reinforced plastic composite. Opt Lasers Eng 51:1125–1132. https://doi.org/10.1016/j.optlaseng.2013.04.017
2. Bhaskar V, Kumar D, Singh KK (2017) Laser processing of glass fiber reinforced composite material: a review. Aust J Mech Eng 4846:1–14. https://doi.org/10.1080/14484846.2017.1363989
3. Altin Karataş M, Gökkaya H (2018) A review on machinability of carbon fiber reinforced polymer (CFRP) and glass fiber reinforced polymer (GFRP) composite materials. Def Technol 14:318–326. https://doi.org/10.1016/j.dt.2018.02.001
4. Gaitonde VN, Karnik SR, Rubio JC, Correia AE, Abrão AM, Davim JP (2008) Analysis of parametric influence on delamination in high-speed drilling of carbon fiber reinforced plastic composites. J Mater Process Technol 203:431–438. https://doi.org/10.1016/J.JMATPROTEC.2007.10.050
5. Che D, Saxena I, Han P, Guo P, Ehmann KF (2014) Machining of carbon fiber reinforced plastics/polymers: a literature review. J Manuf Sci Eng 136:034001. https://doi.org/10.1115/1.4026526
6. Yung KC, Mei SM, Yue TM (2002) A study of the heat-affected zone in the UV YAG laser drilling of GFRP materials. J Mater Process Technol 122:278–285. https://doi.org/10.1016/S0924-0136(01)01177-3
7. Solati A, Hamedi M, Safarabadi M (2019) Comprehensive investigation of surface quality and mechanical properties in CO_2 laser drilling of GFRP composites. Int J Adv Manuf Technol 102:791–808. https://doi.org/10.1007/s00170-018-3164-6
8. Solati A, Hamedi M, Safarabadi M (2019) Combined GA-ANN approach for prediction of HAZ and bearing strength in laser drilling of GFRP composite. Opt Laser Technol 113:104–115. https://doi.org/10.1016/j.optlastec.2018.12.016
9. Fatimah S, Ishak M, Aqida SN (2012) CO_2 laser cutting of glass fiber reinforce polymer composite. IOP Conf Ser Mater Sci Eng 36:012033. https://doi.org/10.1088/1757-899X/36/1/012033
10. Schneider F, Wolf N, Petring D (2013) High power laser cutting of fiber reinforced thermoplastic polymers with cw- and pulsed lasers. Phys Procedia 41:415–420. https://doi.org/10.1016/j.phpro.2013.03.096
11. Patel P, Modi BS, Sheth S, Patel T (2015) Experimental investigation, modelling and comparison of kerfwidth in laser cutting of laser cutting of GFRP. Bonfring Int J Ind Eng Manag Sci 5:55–62. https://doi.org/10.9756/bijiems.8052
12. Patel P, Sheth S, Patel T (2016) Experimental analysis and ANN modelling of HAZ in laser cutting of glass fibre reinforced plastic composites. Procedia Technol 23:406–413. https://doi.org/10.1016/j.protcy.2016.03.044
13. Rao SDB, Sethi A, Das AK (2019) Fiber laser processing of GFRP composites and multi-objective optimization of the process using response surface methodology. J Compos Mater 53:1459–1473. https://doi.org/10.1177/0021998318805139
14. Desai CK, Shaikh A (2012) Prediction of depth of cut for single-pass laser micro-milling process using semi-analytical, ANN and GP approaches. Int J Adv Manuf Technol 60:865–882. https://doi.org/10.1007/s00170-011-3677-8
15. Genna S, Leone C, Lopresto V, Tagliaferri V (2015) An experimental study on the surface mechanisms formation during the laser milling of PMMA. Polym Compos 36:1063–1071. https://doi.org/10.1002/pc.23442
16. Prakash S, Kumar S (2018) Pulse smearing and profile generation in CO2 laser micromachining on PMMA via raster scanning. J Manuf Process 31:116–123. https://doi.org/10.1016/J.JMAPRO.2017.11.003
17. Ağbulut Ü, Ayyıldız M, Sarıdemir S (2020) Prediction of performance, combustion and emission characteristics for a CI engine at varying injection pressures. Energy 197:117257. https://doi.org/10.1016/j.energy.2020.117257
18. Kara F, Karabatak M, Ayyildiz M, Nas E (2020) Effect of machinability, microstructure and hardness of deep cryogenic treatment in hard turning of AISI D2 steel with ceramic cutting. J Mater Res Technol 9:969–983. https://doi.org/10.1016/j.jmrt.2019.11.037
19. Asiltürk I, Çunkaş M (2011) Modeling and prediction of surface roughness in turning operations using artificial neural network and multiple regression method. Expert Syst Appl 38:5826–5832. https://doi.org/10.1016/j.eswa.2010.11.041
20. Ayyıldız M, Çetinkaya K (2017) Predictive modeling of geometric shapes of different objects using image processing and an artificial neural network. Proc Inst Mech Eng Part E J Process Mech Eng 231:1206–1216. https://doi.org/10.1177/0954408916659310
21. Basheer AC, Dabade UA, Joshi SS, Bhanuprasad VV, Gadre VM (2008) Modeling of surface roughness in precision machining of metal matrix composites using ANN. J Mater Process Technol 197:439–444. https://doi.org/10.1016/J.JMATPROTEC.2007.04.121
22. Grzesik W, Brol S (2003) Hybrid approach to surface roughness evaluation in multistage machining processes. J Mater Process Technol 134:265–272. https://doi.org/10.1016/S0924-0136(02)01105-6
23. Kohli A, Dixit US (2005) A neural-network-based methodology for the prediction of surface roughness in a turning process. Int J Adv Manuf Technol 25:118–129. https://doi.org/10.1007/s00170-003-1810-z
24. Sanjay C, Jyothi C (2006) A study of surface roughness in drilling using mathematical analysis and neural networks. Int J Adv Manuf Technol 29:846–852. https://doi.org/10.1007/s00170-005-2538-8

25. Zhang G, Eddy Patuwo B, Hu MY (1998) Forecasting with artificial neural networks: the state of the art. Int J Forecast 14:35–62. https://doi.org/10.1016/S0169-2070(97)00044-7
26. Zain AM, Haron H, Sharif S (2010) Prediction of surface roughness in the end milling machining using artificial neural network. Expert Syst Appl 37:1755–1768. https://doi.org/10.1016/J.ESWA.2009.07.033
27. Zuperl U, Cus F (2003) Optimization of cutting conditions during cutting by using neural networks. Robot Comput Integr Manuf 19:189–199. https://doi.org/10.1016/S0736-5845(02)00079-0
28. Cus F, Zuperl U (2006) Approach to optimization of cutting conditions by using artificial neural networks. J Mater Process Technol 173:281–290. https://doi.org/10.1016/J.JMATPROTEC.2005.04.123
29. Al-Ahmari AMA (2007) Predictive machinability models for a selected hard material in turning operations. J Mater Process Technol 190:305–311. https://doi.org/10.1016/J.JMATPROTEC.2007.02.031
30. Davim JP, Gaitonde VN, Karnik SR (2008) Investigations into the effect of cutting conditions on surface roughness in turning of free machining steel by ANN models. J Mater Process Technol 205:16–23. https://doi.org/10.1016/J.JMATPROTEC.2007.11.082
31. Nalbant M, Gökkaya H, Toktaş İ, Sur G (2009) The experimental investigation of the effects of uncoated, PVD- and CVD-coated cemented carbide inserts and cutting parameters on surface roughness in CNC turning and its prediction using artificial neural networks. Robot Comput Integr Manuf 25:211–223. https://doi.org/10.1016/J.RCIM.2007.11.004
32. Suman S (2020) Deep neural network based prediction of burst parameters for Zircaloy-4 fuel cladding during loss-of-coolant accident. Nucl Eng Technol. https://doi.org/10.1016/j.net.2020.04.025
33. Mustafa A (2019) Modeling for prediction of surface roughness in milling medium density fiberboard with a parallel robot. Sens Rev 39:716–723. https://doi.org/10.1108/SR-02-2019-0051
34. Acherjee B, Mondal S, Tudu B, Misra D (2011) Application of artificial neural network for predicting weld quality in laser transmission welding of thermoplastics. Appl Soft Comput 11:2548–2555. https://doi.org/10.1016/J.ASOC.2010.10.005
35. Piñeiro G, Perelman S, Guerschman JP, Paruelo JM (2008) How to evaluate models: observed versus predicted or predicted versus observed? Ecol Modell 216:316–322. https://doi.org/10.1016/J.ECOLMODEL.2008.05.006
36. Kiseľák J, Lu Y, Švihra J, Szépe P, Stehlík M (2020) "SPOCU": scaled polynomial constant unit activation function. Neural Comput Appl. https://doi.org/10.1007/s00521-020-05182-1
37. Shyha I (2013) An investigation into CO_2 laser trimming of CFRP and GFRP composites. Procedia Eng 63:931–937. https://doi.org/10.1016/j.proeng.2013.08.200